

Article

Discrimination of Clinozoisite–Epidote Series by Raman Spectroscopy: An application to Bengal Fan Turbidites (IODP Expedition 354)

Mara Limonta ^{1,2} , Sergio Andò ^{1,*} , Danilo Bersani ³  and Eduardo Garzanti ¹ 

¹ Laboratory for Provenance Studies, Department of Earth and Environmental Sciences, University of Milano-Bicocca, 20126 Milano, Italy

² Centre de Recherches Pétrographiques et Géochimiques, Université de Lorraine-CNRS, 54501 Vandœuvre-lès-Nancy, France

³ Department of Mathematical, Physical and Computer Sciences, University of Parma, 43124 Parma, Italy

* Correspondence: sergio.ando@unimib.it

Abstract: Epidote group minerals are one of the three most abundant kinds of heavy minerals in orogenic sediments, the other two being amphibole and garnet. They resist diagenesis better than amphibole and resist weathering in soils better than garnet. Their chemical composition and optical properties vary markedly and systematically with temperature and pressure conditions during growth. Useful information on the metamorphic grade of source rocks can thus be obtained by provenance analysis. In this study, we combine optical, SEM–EDS, and Raman analyses of nine standard crystals of epidote group minerals collected from different rock units exposed in the European Alps and Apennines and develop a Raman library for efficient discrimination of epidote, clinozoisite, zoisite, and allanite by establishing clear user-oriented relationships among optical properties, chemical composition, and Raman fingerprint. This new library allows us to distinguish and reliably determine, directly from their Raman spectrum, the chemical compositions of epidote group minerals during routine heavy mineral analyses of sand/sandstone and silt/siltstone samples down to the size of a few microns. The validity of the approach is illustrated by its application to 41 Bengal Fan turbidites collected from five cores during IODP Expedition 354 and ranging in grain size from medium sand to fine silt.

Keywords: provenance analysis; Raman spectroscopy; heavy minerals; zoisite; allanite; Himalayan orogen; Bengal Fan



Citation: Limonta, M.; Andò, S.; Bersani, D.; Garzanti, E. Discrimination of Clinozoisite–Epidote Series by Raman Spectroscopy: An application to Bengal Fan Turbidites (IODP Expedition 354). *Geosciences* **2022**, *12*, 442. <https://doi.org/10.3390/geosciences12120442>

Academic Editors: Andrew C. Morton and Jesus Martinez-Frias

Received: 5 October 2022

Accepted: 22 November 2022

Published: 1 December 2022

Publisher's Note: MDPI stays neutral with regard to jurisdictional claims in published maps and institutional affiliations.



Copyright: © 2022 by the authors. Licensee MDPI, Basel, Switzerland. This article is an open access article distributed under the terms and conditions of the Creative Commons Attribution (CC BY) license (<https://creativecommons.org/licenses/by/4.0/>).

1. Introduction

Varietal studies of single detrital mineral species integrated using bulk petrography and heavy mineral data place fundamental constraints on the provenance analysis of modern sediments and ancient sedimentary rocks [1–3]. Raman spectroscopy is a powerful tool to accurately characterize mineralogical species and to improve our understanding of the sedimentary processes that modify provenance signals during sediment transfer from source to sink [4,5]. Raman spectroscopy is an efficient and non-destructive technique which has an excellent spatial resolution (down to a few μm ; e.g., [6,7]) and does not require specific sample preparation [8–10], potentially making it suitable to replace other techniques such as QemScan and MLA [11–13], or other analytical tools (e.g., XRD). Notwithstanding its potential, Raman spectroscopy has been mainly used in a semi-quantitative way in the Earth Sciences until recently, and only on a limited number of selected minerals. Raman spectroscopy studies aimed at identifying the chemical composition of specific detrital minerals in relationship with the lithology of their source rocks have been dedicated to garnet [10], amphibole [14], pyroxene [15], titanite [16], and rutile [17]. Microprobe, X-ray, Raman, and infrared spectroscopy analyses have been applied for the chemical

characterization of different epidote group minerals [18–21] and to identify their source rocks [22–24], but a quantitative study on their Raman fingerprints has not so far been carried out.

This study contributes to the filling of the existing knowledge gap concerning the identification of epidote group minerals in sediments, with the main aim of assessing the relationship between their composition and their parent rocks. Here we will focus on detrital epidote, clinozoisite, zoisite, and allanite, which are the most common detrital species derived from igneous and metamorphic rocks [23,25–28]. Zoisite, an orthorhombic polymorph of clinozoisite, is here considered as part of the epidote group (although it does not strictly belong to it [29]) because its optical properties are similar to those of the epidote–clinozoisite series and because it is an important provenance tracer for high-pressure source rocks. Epidote group minerals are ubiquitous in orogenic sediments [30] and, being moderately durable during both weathering and diagenesis, are widespread in sediments of Cenozoic age [31–34].

In this study, we combine optical, SEM–EDS, and Raman analyses of nine standard crystals collected from different rock units exposed in the European Alps and northern Apennines and develop a new Raman library for epidote group minerals by establishing clear user-oriented relationships among optical properties (e.g., pleochroism and birefringence), chemical composition (e.g., relative amounts of Fe and Al), and Raman fingerprint (i.e., position of principal and secondary peaks). The Raman reference spectra allow us to routinely classify the different minerals found in sand- and silt-sized sediments and to reliably determine their chemical composition from their Raman signal directly on grain mounts or from thin sections, with no need to resort to techniques involving more complex preparation procedures. The validity of this approach is illustrated by its application to Bengal Fan turbidites. A precise assessment of the relative amount of diverse detrital epidote group minerals provides information on the metamorphic grade of source rocks, complementary to that obtained by classical petrographic and heavy mineral analyses and useful to reconstruct the erosional evolution of the Himalayan orogen through the last 20 Ma.

2. Epidote Group Minerals

Epidote group minerals are monoclinic sorosilicates described with the general formula $A_2M_3[T_2O_7][TO_4](O,F)(OH,O)$, and their topology is consistent with space group $P2_1/m$. The key cation sites $-A = Ca, Sr, Pb, REE^{3+}$, $M = Al, Fe^{3+}, Mn^{3+}, Mg, Fe^{2+}, Mn^{2+}, Cr, V$, and $T = Si$ determine their root name [29]. The chemical composition of epidote group minerals is highly variable and reflects crystallization conditions (e.g., temperature, pressure, oxygen fugacity, and bulk rock composition), thus reflecting the characteristics and metamorphic grade of source rocks [26,35,36].

Epidote $\{Ca_2Al_2Fe^{3+}[Si_2O_7][SiO_4]O(OH)\}$ is typical of greenschist facies metamorphic rocks, where it is associated with albite, actinolite, and chlorite, but it also occurs in intermediate to mafic amphibolite facies rocks associated with plagioclase and hornblende. Epidote forms from a variety of protoliths, including mixed siliciclastic–carbonate sediments and mafic to intermediate magmatic rocks [22,27,36], under a variety of temperature gradients, and from medium to high, and even ultrahigh, pressure regimes [26,37]. Commonly associated with glaucophane in blueschist facies metamorphic rocks [38], it may also be the product of the metasomatic alteration of pyroxene, amphibole, and plagioclase in magmatic rocks [39].

Clinozoisite $\{Ca_2Al_3[Si_2O_7][SiO_4]O(OH)\}$ is characteristic of low- to medium-grade metamorphic rocks (i.e., greenschist and epidote–amphibolite facies), and commonly occurs in association with actinolite, but it also occurs in blueschists facies mafic rocks. Zoisite $\{Ca_2Al_3[Si_2O_7][SiO_4]O(OH)\}$ is typical of regional metamorphism, being a relatively common constituent of epidote–amphibolite facies rocks derived from calcareous shales and sandstones as well as amphibolites derived from mafic igneous rocks, as in eclogites and blueschists [38]. It also occurs in calc–silicate granulites and calcite–zoisite micaschists [1].

Allanite $\{Ca_2(REE)^{3+}Al_2Fe^{2+}[Si_2O_7][SiO_4]O(OH)\}$ incorporates light rare earth elements (LREE) as well as Th [40–43], making it a mineral that is potentially economically valuable and frequently slightly radioactive. Allanite is relatively common in granite, granodiorite, monzonite, and syenite, and it may occur also in pegmatite and limestone skarn [38,44].

Some chemical properties of epidote group minerals can be deduced from optical properties (e.g., optical sign; pleochroism, birefringence) determined during routine heavy mineral counting. Pleochroism is related to the degree of Al, Fe^{3+} substitution, and it is strong in iron-rich deep yellowish green epidote grains and weak in iron-poor, colorless to pale yellowish green clinozoisite [29]. However, optical properties depend on crystallographic orientation and are insufficient to allow a precise assessment of the geochemical composition of detrital epidote group minerals [1].

Zoisite is commonly colorless, with greyish white or anomalous indigo-blue and yellow interference colors and parallel extinction. Allanite has strong greenish brown to reddish brown pleochroism and second-order interference colors, which may make it similar to reddish brown hornblende or dark brown dravitic tourmaline [45].

2.1. The Epidote–Clinozoisite Series

Epidote and clinozoisite are the two end members of the epidote–clinozoisite series. Solid solutions are distinguished by the ratio between iron and aluminum ($X_{Fe} = Fe^{3+} / (Fe^{3+} + Al)$) and are optically negative if Fe-rich (epidote) and optically positive if Al-rich (clinozoisite). The X_{Fe} value tends to decrease with increasing metamorphic grade [26,27], and the appearance of clinozoisite marks the transition from the very low to the low metamorphic grade [46]. The X_{Fe} ranges in epidote from 13.6 to 53.3 (Fe_2O_3 7.6–23.4; $FeO \leq 0.8$; Al_2O_3 13.1–30.9) and in clinozoisite from 0.2 to 13.1 (Fe_2O_3 0.6–6.4; FeO 1.1–1.8; Al_2O_3 27.8–30.7; [38]). In zoisite, X_{Fe} does not exceed 0.15, and it is mostly ≤ 0.074 (Fe_2O_3 0.04–3.97; $FeO \leq 0.4$; Al_2O_3 32.0–33.5; [38,47]). The change from optically negative epidote to optically positive clinozoisite has been considered to occur at Ep 30% (6 wt% Fe_2O_3 ; [38,48]), at Ep 35% [47], or at Ep 40% [29].

2.2. Raman Analysis of Epidote Group Minerals

Raman spectroscopy has rarely been applied to estimate the chemical composition of epidote group minerals, in particular by considering the diagnostic peaks in the low-frequency region of the spectral range (i.e., 150–1200 cm^{-1} ; [20,49,50]). Nagashima et al. [51] took into account the OH-stretching peak in the high-frequency region (3200–3600 cm^{-1}) and observed that stretching modes shift toward higher wavenumbers with increasing Fe content. In the low-frequency region, the Raman spectrum of epidote is characterized by an abundance of intense peaks at about 400 cm^{-1} to 420 cm^{-1} , 550 cm^{-1} , 910 cm^{-1} , and 1080 cm^{-1} , and by a lack of peaks between 600 cm^{-1} and 820 cm^{-1} [49], which facilitates distinction from other silicates [5]. Clinozoisite displays diagnostic peaks at about 980 cm^{-1} and 1090 cm^{-1} originating from Si–O bond-stretching modes, and a peak at 570 cm^{-1} associated with a Si–O–Si bending mode [51]. The zoisite spectrum is distinguished by an intense peak at 490 cm^{-1} related to a Si–O bending mode, and by other peaks at about 680 cm^{-1} , 870 cm^{-1} , 1070 cm^{-1} , and 1091 cm^{-1} [50].

3. Materials and Methods

For this study, the following mineral standards were used: six in the epidote–clinozoisite series (E1, E2, E3, E4 and C1, C2 [52–55]), one zoisite (Z [5]), and two allanites-(Ce) (A1 and A2 [55,56]). These standards were collected from different localities in the European Alps and Apennines (Supplementary File S1, Table S1) and selected to cover a wide range of compositions and metamorphic grade of source rocks and to define the limit between epidote and clinozoisite based on Raman spectroscopy data. Mineral standards were crushed in an agate mortar. The fragments were mounted on a Huntsman Araldite® DBF resin stub, cut, and polished to perform optical, scanning electron microscopy (SEM), energy dispersive spectroscopy (EDS), and Raman spectroscopy analyses on different fragments

of the very same crystal. Several points were analyzed for each standard, first by Raman spectroscopy and then by SEM–EDS on the same spot.

The correlation of Raman spectra and SEM–EDS analyses allowed us to discriminate among epidote group minerals in the grain mounts of 41 Bengal Fan turbidite samples collected from five cores drilled during IODP Expedition 354 [57]. After separation by centrifuging in Na-polytungstate (density 2.90 g/cm^3), following [58,59], heavy mineral analyses were carried out on the 15–500 μm (for sand) or $>5 \mu\text{m}$ (for silt) size classes obtained by wet sieving. About 50 Raman spectra of detrital epidote group minerals were collected on each heavy mineral slide. Full information on core locations, sample age and grain size, heavy mineral data, and Raman peaks in the OH region for each of the five studied Bengal Fan cores is provided in Supplementary File S2 [60,61]. Provenance analysis based on integrated petrographic and mineralogical data is illustrated in [62].

3.1. SEM–EDS Mineral Chemistry

Mineral standards were coated with graphite and analyzed for major elements at the PMiB (University of Milano-Bicocca, Milano, Italy) with a Tescan VEGATM TS Univac 5136 XM scanning electron microscope coupled with an EDAX GenesisTM 4000 XMS Imaging 60 SEM–EDS under an electron beam with a high voltage of 20 kV, 250-nm spot size, and current absorption $190 \text{ pA} \pm 1 \text{ pA}$, measured in a platinum Faraday cup. The quantification of main and trace elements (Si, Al, Ca, Fe, Mg, Mn, and REE) was calibrated according to Astimex Scientific standards. Because of crystal zoning, compositional variability turned out to be stronger in the epidote standard E3. All SEM–EDS analyses of mineral standards are provided in Table S2.

3.2. Raman Spectroscopy

Optical techniques represent the fundamental and classic approach to investigating the mineralogical composition of sediments [1,63]. A first discrimination among epidote group minerals can be obtained based on relief, pleochroism, anomalous birefringence colors, angle between optical axes, and optical sign (Figure 1). This task, however, becomes challenging in silt or with grains not showing their prismatic face {100} on the slide. Raman spectroscopy does not only offer a quick method to solve these problems, but represents a very efficient tool to obtain quantitative compositional data.

Raman spectra for the nine mineral standards were collected at the Laboratory for Provenance Studies (University of Milano-Bicocca, Milano, Italy) by a high-resolution Renishaw inViaTM Reflex confocal Raman microscope, equipped with a Leica DM2500 polarizing microscope with objectives up to $100\times$ and motorized x–y stage. The system was calibrated using the 520.7 cm^{-1} Raman peak of silicon. Spectra were obtained using the $50\times$ LWD (long working distance) objective and a 532-nm line, solid-state laser with a power of 10 mW at the sample controlled by density filters to avoid heating effects. The acquisition time was 60 s and the spectral resolution was 1 cm^{-1} .

The minimum lateral resolution of the laser was 2 μm and the depth resolution was a few μm . We considered the low wavenumber range ($140\text{--}1200 \text{ cm}^{-1}$) and in particular the high wavenumber range ($3000\text{--}3800 \text{ cm}^{-1}$), which turned out to be crucial for detecting the OH-stretching signal. The Renishaw WIRE software package was used for baseline subtraction and to perform the spectral deconvolution using Gauss-Lorentzian functions and determine the position of the Raman peaks.

Between two and eleven spectra were collected for each mineral standard (Figure 2), and photos with the analyzed Raman spots were taken to carry out SEM–EDS analyses in exactly the same spots (Figure 3). The diagnostic peaks of the epidote–clinozoisite standards are provided in Table S3.

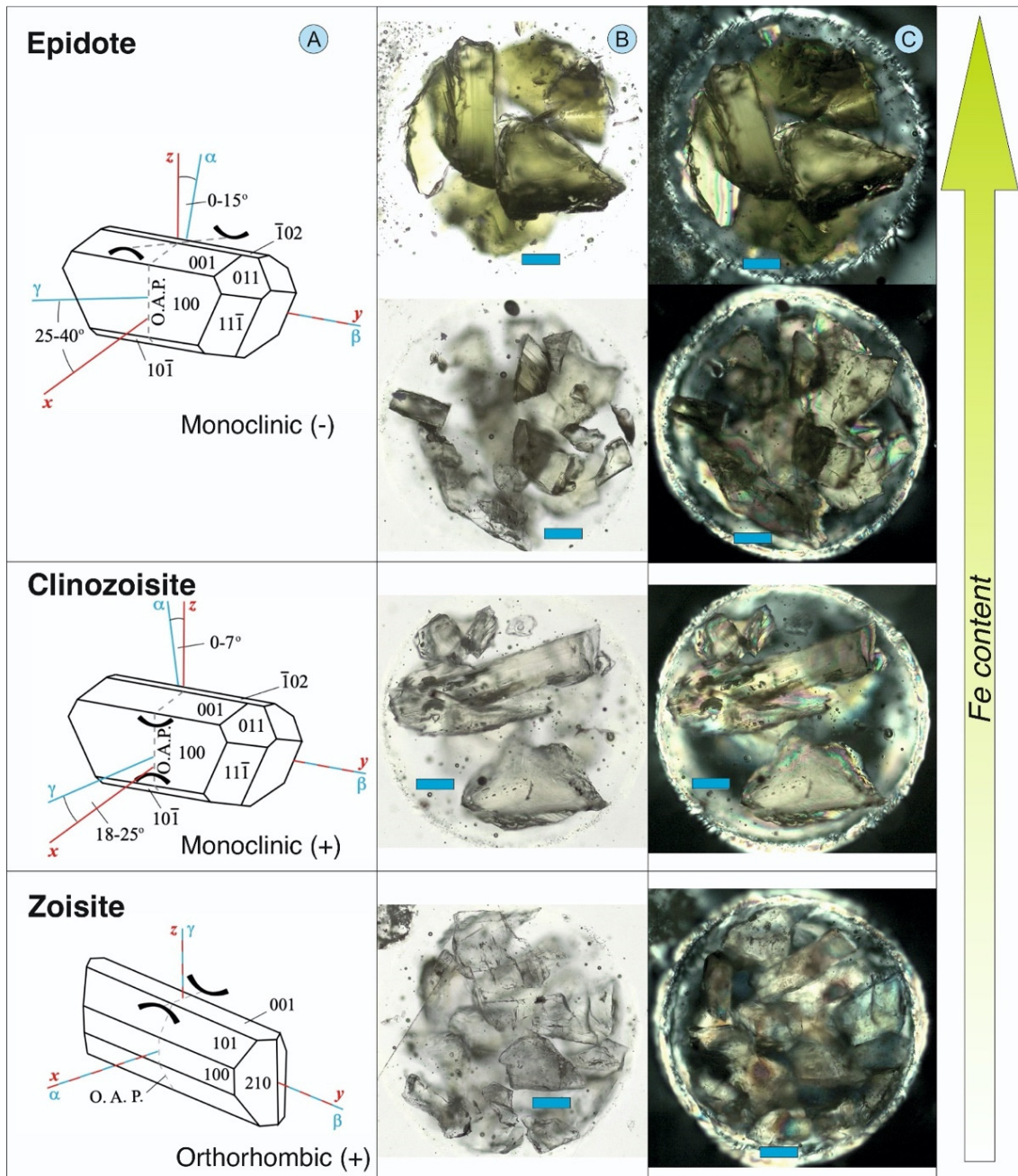


Figure 1. Optical features. (A) Epidote group minerals are biaxial with an optical axis perpendicular to the elongation of the crystal. The optical sign is negative in epidote and positive in clinozoisite and zoisite (modified after [63]). (B) Parallel-polarized light: pleochroism increases with iron content from colorless clinozoisite to yellowish green epidote. Zoisite is colorless. (C) Cross-polarized lights: birefringence increases with iron content in the epidote–clinozoisite series. Zoisite shows anomalous indigo-blue and yellow interference colors. Shown in (B,C) are fragments of standards E1, E3, C1, and Z. Blue bar for scale = 100 μ m.

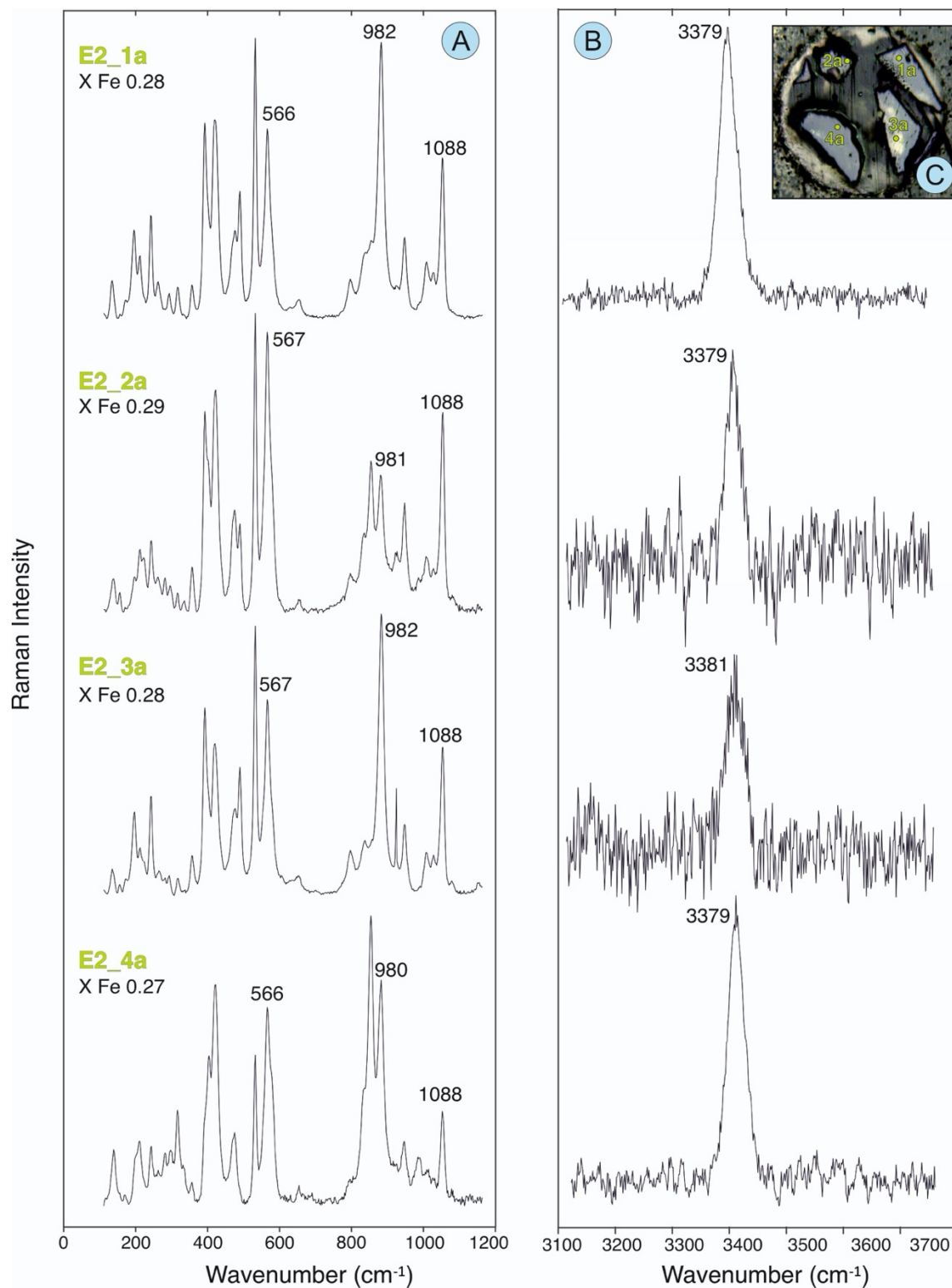


Figure 2. Characterization of epidote standard E2. Raman spectra in the low-frequency (A) and high-frequency (B) regions. (C) Map of the analyzed points in four crystal fragments (note the minor variability in the positions of the Raman peaks and of the X_{Fe} values determined by SEM-EDS).

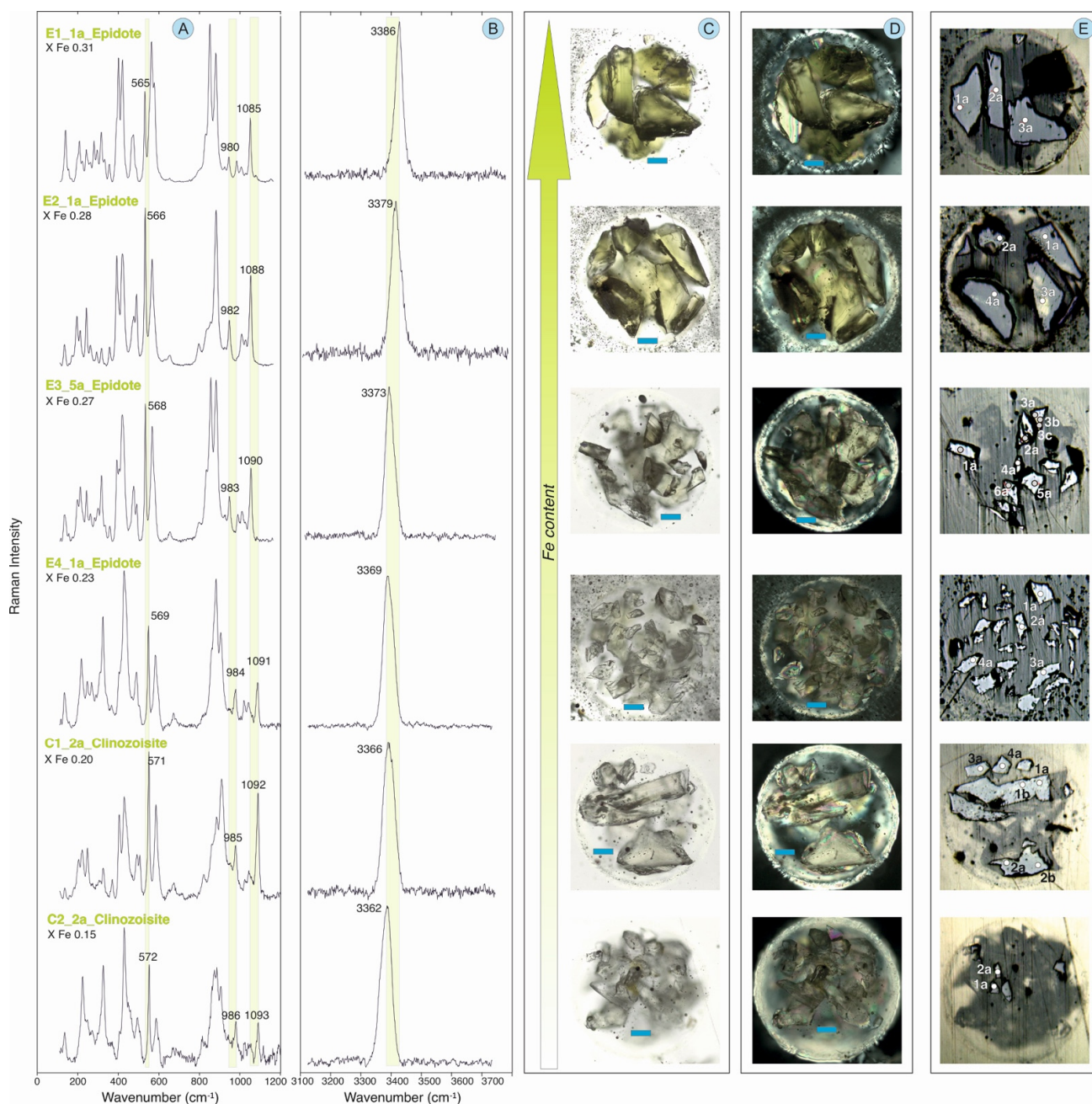


Figure 3. Characterization of epidote and clinozoisite standards. Diagnostic Raman peaks in the low-frequency (A) and high-frequency OH (B) regions. (C) Increase in pleochroism with increasing iron content. (D) Increase in birefringence with increasing iron content. (E) Maps of analyzed points. Blue bar for scale = 100 μm .

4. SEM–EDS and Raman Analyses of Mineral Standards

Epidote contains up to 14.0 wt% FeO_t and clinozoisite up to 29.3 wt% Al_2O_3 . Zoisite contains only 2.2–2.7 wt% FeO_t , but up to 31.7 wt% Al_2O_3 . In allanite, FeO_t ranges from 4.4 wt% to 13.5 wt%, and Al_2O_3 from 15.9 wt% to 20.1 wt%, with up to 20 wt% accounted for by La_2O_3 , Ce_2O_3 , Pr_2O_3 , Nd_2O_3 , UO_2 , and ThO_2 .

The Raman spectra of mineral standards display many peaks in the low-frequency region (140–1200 cm^{-1}) and one intense peak related to the OH-stretching vibration in the high-frequency region (3000–3600 cm^{-1}). The epidote–clinozoisite series is characterized by intense peaks at about 400 cm^{-1} to 420 cm^{-1} , 570 cm^{-1} , 910 cm^{-1} , and 1080 cm^{-1} , a lack of peaks between 600 cm^{-1} and 820 cm^{-1} (Figure 3A), and a high wavenumber

peak between 3350 cm^{-1} and 3390 cm^{-1} (Figure 3B). Peaks up to $200\text{--}250\text{ cm}^{-1}$ are related to translations of cations or anionic groups, peaks between 275 cm^{-1} and 300 cm^{-1} are related to Ca-O-stretching vibrations, peaks in the ranges $300\text{--}400\text{ cm}^{-1}$ and $500\text{--}550\text{ cm}^{-1}$ are related to Al-O- or Fe-O-stretching vibrations, peaks in the ranges $430\text{--}450\text{ cm}^{-1}$ and $565\text{--}580\text{ cm}^{-1}$ are related to Si-O_b-Si bending, the peak near 600 cm^{-1} is related to Si-O_b stretching, and the peaks between 830 and 1100 cm^{-1} are related to Si-O_{nb} stretching [64]. Zoisite is identified by a major peak at 490 cm^{-1} related to the Si-O-bending mode [50], by secondary peaks at about 680 cm^{-1} , 870 cm^{-1} , 1070 cm^{-1} , and 1091 cm^{-1} , and by the high wavenumber peak at about 3150 cm^{-1} (Figure 4A). Allanite is singled out by one sharp major peak at 689 cm^{-1} and displays several wide overlapping peaks in the high-frequency region (Figure 4B).

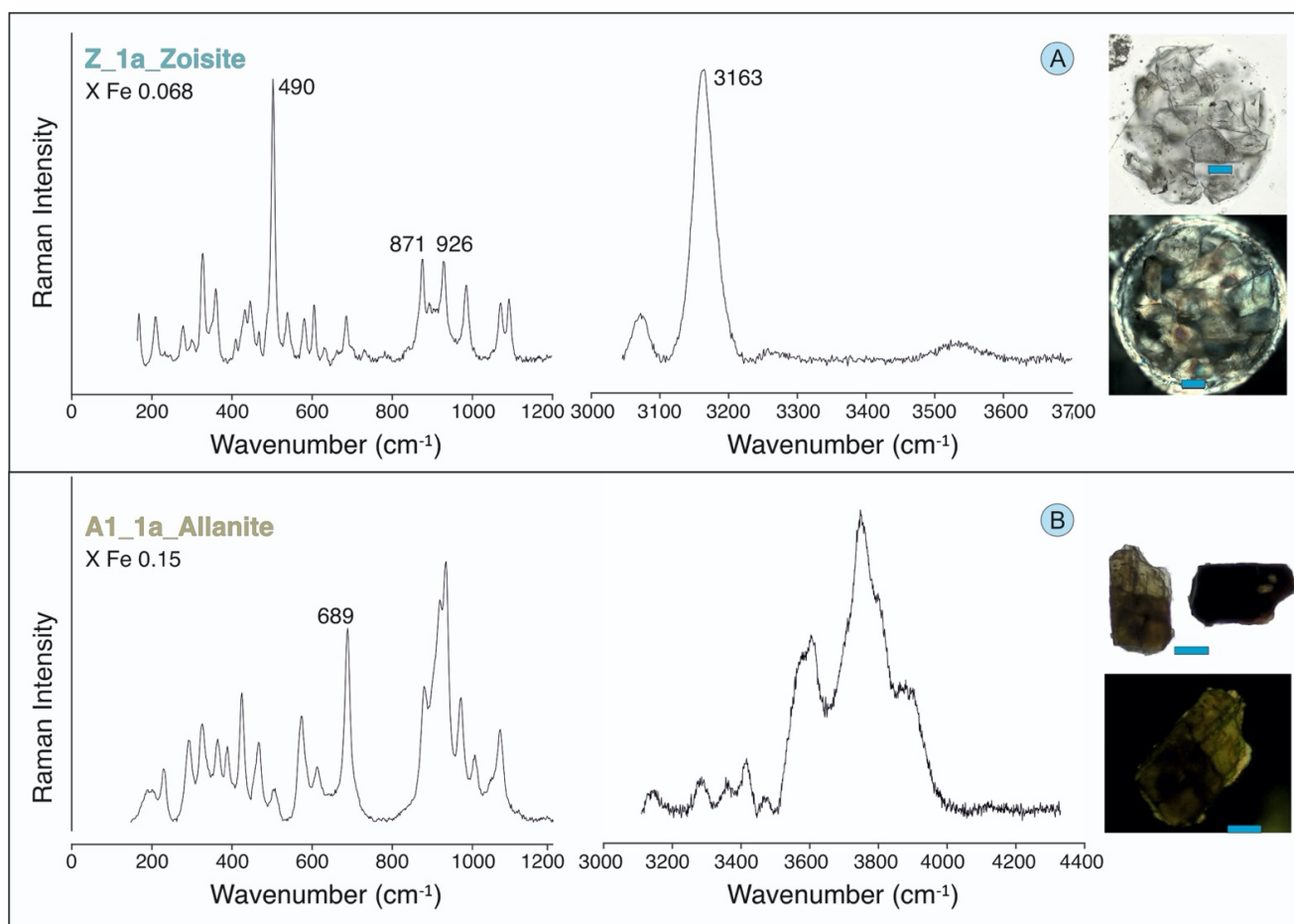


Figure 4. Characterization of zoisite and allanite standards Z (A) and A1 (B). Zoisite, identified by major Raman peaks at 490 cm^{-1} and $\sim 3150\text{ cm}^{-1}$, is colorless, with anomalous interference colors. Allanite, identified by a sharp peak at 689 cm^{-1} and several wide peaks in the high-frequency region, has strong pleochroism and second-order interference colors. Blue bar for scale = $100\text{ }\mu\text{m}$.

4.1. How to Calculate X_{Fe} in the Epidote–Clinzoisite Series

The progressive substitution of Fe^{2+} with Al^{3+} determines a progressive red shift of the main Raman peaks in the low-frequency region (Figure 3A) and a blue shift in the high-frequency region (Figure 3B). Such a progressive shift can be fitted by a linear interpolation of the X_{Fe} values obtained by SEM–EDS with the three strongest Raman peaks in the low-frequency region (ν_1 : $565\text{--}573\text{ cm}^{-1}$, ν_2 : $980\text{--}987\text{ cm}^{-1}$, ν_3 : $1085\text{--}1096\text{ cm}^{-1}$) and the main peak in the high-frequency region (ν_4 : $3386\text{--}3360\text{ cm}^{-1}$).

By using the three low-wavenumber peaks, which are all well separated from the other peaks, three well defined equations are obtained (Figure 5):

$$X_{\text{Fe}} = -0.022301 \nu_1 + 12.915 \quad (R^2 = 0.90)$$

$$X_{\text{Fe}} = -0.025055 \nu_2 + 24.868 \quad (R^2 = 0.84)$$

$$X_{\text{Fe}} = -0.017607 \nu_3 + 19.434 \quad (R^2 = 0.86)$$

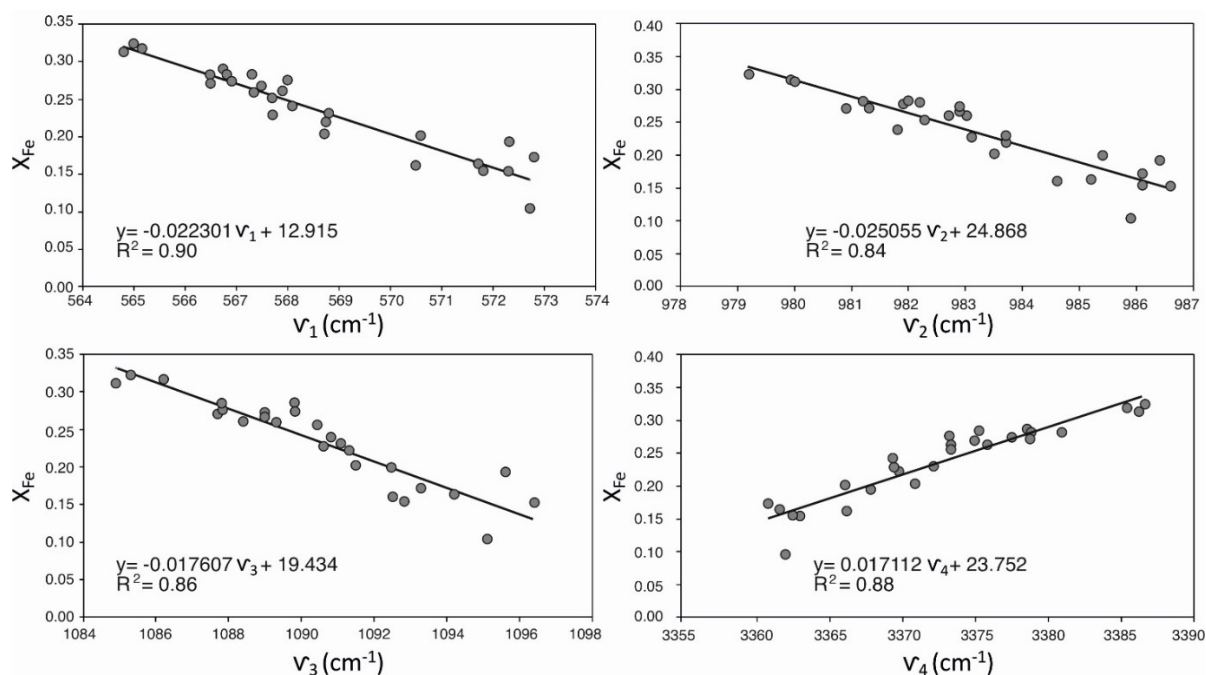


Figure 5. Correlation between Raman peak positions and chemical composition (X_{Fe} determined by SEM-EDS) in the six epidote and clinozoisite standards.

The OH-vibration mode at high wavenumber is a couplet including a higher peak and a shoulder that progressively disappears with increasing X_{Fe} . The equation obtained by the deconvolution of the overlapping peak and shoulder using a combination of Lorentzian and Gaussian functions is:

$$X_{\text{Fe}} = 0.007112 \nu_4 - 23.752 \quad (R^2 = 0.88, \text{ Figure S1}).$$

The MATLAB™ program “*epidotefull*” was developed to estimate X_{Fe} by combining the compositional information provided by the four Raman peaks, considered as input. The average of the X_{Fe} values obtained by the four equations, weighted by their R^2 value, is taken as the best estimate of the X_{Fe} of the mineral. The calculations are based on all four main Raman peaks (ν_1 , ν_2 , ν_3 , and ν_4), and the result is very sensitive to the exact value of the coefficient of the wavenumber, so it is recommended to use all the shown digits for the calculations. The presence of minor or trace amounts of Mg, Mn, Cr, and V can cause small shifts in the Raman spectrum, but their impact is not likely to cause a misidentification of epidote/clinozoisite. Such small chemical variations can indeed influence the calculation of the X_{Fe} , but this effect it is taken into account in the uncertainty associated with the method and is reduced by combining different peaks. A detailed description of the program “*epidotefull*” is provided as Supplementary File S3.

4.2. Distinguishing Epidote from Clinozoisite

Whereas zoisite and allanite are readily identified by their diagnostic peaks at about 490 cm⁻¹ and 689 cm⁻¹, respectively, discrimination within the epidote–clinozoisite series requires additional care. The boundary between optically negative epidote and optically positive clinozoisite is only broadly defined in the Ep₃₀ (X_{Fe} 0.20) to Ep₄₀ (X_{Fe} 0.27) range. In

this study, we adopted the Ep_{30} value recommended by [38], which separates the optically negative standards E1, E2, E3, and E4 from the optically positive standards C1 and C2. Based on the combined SEM–EDS and Raman analyses, the boundary between epidote and clinozoisite is thus established at FeO_{tot} 8 wt%, X_{Fe} 0.20, ν_1 570 cm^{-1} , ν_2 984 cm^{-1} , ν_3 1092 cm^{-1} , and ν_4 3369 cm^{-1} (Table 1).

Table 1. Total iron content determined by SEM–EDS, X_{Fe} values, and position of Raman peaks ν_1 , ν_2 , ν_3 , and ν_4 for the six epidote and clinozoisite standards.

Sample	FeO_t	X_{Fe}	ν_1 (cm^{-1})	ν_2 (cm^{-1})	ν_3 (cm^{-1})	ν_4 (cm^{-1})
E1	13.5–14.0	0.31–0.32	565	979–980	1085–1086	3385–3386
E2	11.7–11.9	0.27–0.29	566–567	981–982	1088	3379–3381
E3	10.6–11.9	0.23–0.28	567–568	981–983	1088–1091	3372–3378
E4	9.2–10.0	0.20–0.24	568–569	982–984	1091–1092	3369–3371
C1	6.3–7.9	0.15–0.16	570–572	985–986	1092–1093	3362–3366
C2	4.5–8.0	0.10–0.20	571–573	985–987	1094–1096	3361–3368

5. Epidote Group Minerals in the Bengal Fan

Bengal Fan turbidites collected from cores U1454, U1453, U1452, U1449, and U1451 during IODP Expedition 354 and ranging from fine silt to medium sand (9 μm to 300 μm ; 6.9 ϕ to 1.7 ϕ) have provided an excellent opportunity to test the usefulness in provenance analysis of the Raman approach illustrated above. Epidote group minerals, including mainly Fe-rich epidote with subordinate clinozoisite and rare zoisite and allanite, represent $14\% \pm 4\%$ of the rich to moderately rich transparent heavy mineral (tHM) suites of the Quaternary turbidites and $24\% \pm 3\%$ of the moderately poor tHM suites of the Zanclean–Tortonian strata, reaching up to 30% of the poor tHM suite of the lowermost Miocene sample (Table 2). Such a relative increase in relatively durable epidote group minerals in older strata containing depleted tHM suites is ascribed to selective dissolution of amphibole and other less chemically resistant minerals during diagenesis [62]. Relative to the bulk sample, the content of epidote group minerals remains approximately constant ($0.6\% \pm 0.3\%$) in strata buried less than 500 m and as old as 8 Ma (Late Miocene), but progressively decreases in older and more deeply buried strata from core U1451, where epidote group minerals also start to be selectively dissolved (yet at a much lower rate than amphibole).

Quaternary samples from the five studied Bengal Fan cores show no significant difference in the relative abundance of epidote group minerals (Figure 6). Fe-rich epidote represents $65\% \pm 9\%$, and clinozoisite represents $30\% \pm 10\%$, with minor zoisite (mostly < 10% but locally up to 28%) and allanite (mostly < 5% but locally up to 12%). Older samples from core U1451 do not show marked differences, clinozoisite reaching its maximum (41%) in a Pliocene turbidite and allanite reaching its maximum (8%) in the oldest, lowermost Miocene turbidite.

The Raman-determined X_{Fe} values of detrital epidote and clinozoisite are also similar in all Quaternary samples, showing a mode between 0.25 and 0.3 (i.e., close to the epidote/clinozoisite boundary; Figure 7). The proportion between epidote and clinozoisite and also X_{Fe} values do not change notably in older strata, suggesting that the provenance signal carried by epidote group minerals is not markedly affected by selective diagenetic dissolution of Fe-rich vs. Fe-poor grains.

Table 2. Average composition of detrital epidote group minerals in turbidites of different ages from the five studied Bengal Fan cores, as determined using the new Raman library (**mean** in bold, *standard deviation* in italics); n°, number of analyzed grains; tHM, transparent heavy minerals; EpGM, epidote group minerals; Ep, epidote; Czo, clinozoisite; Zo, zoisite; Aln, allanite; RF Ep, epidote-bearing rock fragments.

Core Site	Depth (m)	Age	n°	tHM%	% EpGM	%Ep	%Czo	%Zo	%Aln	%Ep RF	XFe
U1454B	30-160	Quaternary	203	6.3 <i>3.6</i>	16 <i>6</i>	65 <i>7</i>	28 <i>12</i>	1 <i>2</i>	3 <i>4</i>	3 <i>4</i>	0.24 <i>0.06</i>
U1453A	20-190	Quaternary	177	3.8 <i>1.0</i>	12 <i>1</i>	66 <i>14</i>	26 <i>19</i>	7 <i>10</i>	1 <i>2</i>	0 <i>0</i>	0.24 <i>0.06</i>
U1452B	50-190	Quaternary	160	4.8 <i>1.6</i>	15 <i>1</i>	64 <i>12</i>	30 <i>10</i>	2 <i>3</i>	2 <i>2</i>	2 <i>4</i>	0.24 <i>0.07</i>
U1449A	8-208	Quaternary	212	3.5 <i>0.9</i>	17 <i>2</i>	68 <i>9</i>	31 <i>6</i>	1 <i>2</i>	1 <i>1</i>	0 <i>0</i>	0.24 <i>0.06</i>
U1451A	25-117	Quaternary	167	4.0 <i>0.6</i>	12 <i>4</i>	63 <i>9</i>	33 <i>6</i>	3 <i>3</i>	1 <i>1</i>	0 <i>0</i>	0.24 <i>0.06</i>
U1451A	161	Pliocene	49	1.7	25	57	41	2	0	0	0.21 <i>0.05</i>
U1451AB	200-658	Late Miocene	340	1.7 <i>0.8</i>	24 <i>3</i>	66 <i>4</i>	31 <i>6</i>	2 <i>1</i>	1 <i>2</i>	0 <i>0</i>	0.24 <i>0.07</i>
U1451B	969	Early Miocene	36	0.7	18	61	36	3	0	0	0.23 <i>0.08</i>
U1451B	1027	Early Miocene	62	0.6	30	63	26	3	8	0	0.26 <i>0.07</i>

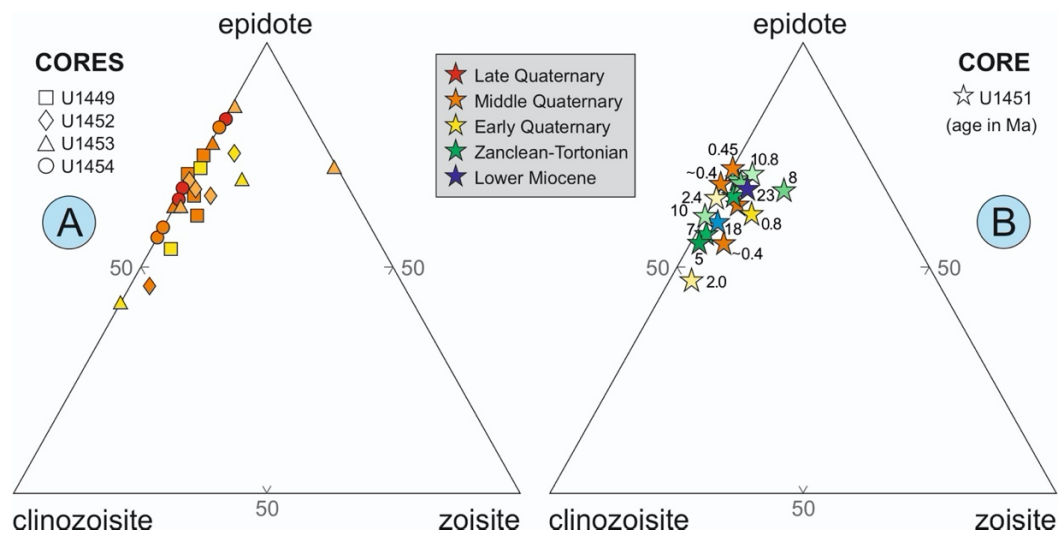


Figure 6. Relative abundance of epidote, clinozoisite, and zoisite in Bengal Fan turbidites. (A) Quaternary samples. (B) Miocene-Pleistocene samples from core U1451 (depositional ages are indicated) show no systematic variability with age and burial depth.

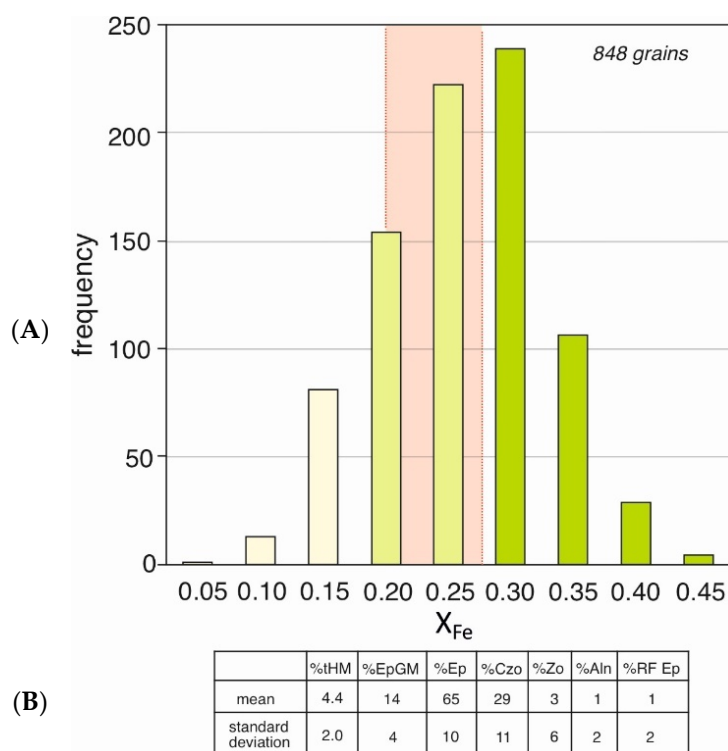


Figure 7. Epidote group minerals in Quaternary Bengal Fan turbidites. (A) Distribution of X_{Fe} values as determined for 848 grains using the new Raman library. The pink rectangle marks the transition between optically negative epidote ($Ep > 30$; $X_{Fe} > 0.27$) and positive clinozoisite ($Ep < 30$; $X_{Fe} < 0.20$). Intermediate values were assigned to epidote if $\nu_4 \geq 3369 \text{ cm}^{-1}$ and to clinozoisite if $\nu_4 < 3369 \text{ cm}^{-1}$. (B) Average composition: tHM, transparent heavy minerals; EpGM, epidote group minerals; Ep, epidote; Czo, clinozoisite; Zo, zoisite; Aln, allanite; RF Ep, epidote-bearing rock fragments.

6. Conclusions

Epidote group minerals, being one of the most abundant heavy minerals in sediments, resisting diagenesis better than amphibole and resisting weathering in soils better than garnet, are among the most useful mineral tracers in varietal studies. For this reason, we developed a new Raman library to objectively distinguish among epidote, clinozoisite, zoisite, and allanite grains by coupling optical observations, SEM–EDS chemical analyses, and Raman spectra obtained for nine standard crystals of epidote group minerals collected from different rock units exposed in the European Alps and northern Apennines. We show how accurate information on the chemical composition of epidote group minerals can be obtained by Raman spectroscopy directly on grain mounts or from thin sections in a few seconds and with no additional sample preparation. Iron content is determined by considering the position of the intense diagnostic Raman peaks in the low-frequency (vibrational modes ν_1 at ca 570 cm^{-1} , ν_2 at ca 980 cm^{-1} , and ν_3 at ca 1090 cm^{-1}) and high-frequency OH region (ν_4 at ca 3370 cm^{-1}). This approach was tested on Bengal Fan turbidites where the relative abundance of epidote, clinozoisite, zoisite, and allanite was identified in sediment ranging in size from medium sand to fine silt ($9 \mu\text{m}$). Quaternary Bengal Fan turbidites contain $65\% \pm 9\%$ of Fe-rich epidote, $30\% \pm 10\%$ clinozoisite, and minor zoisite and allanite. Epidote group minerals remain chiefly unaffected by diagenetic dissolution in strata buried less than 500 m and as old as 8 Ma. In older and more deeply buried strata, epidote and clinozoisite start to be dissolved, but their ratio remains constant, suggesting that it can be profitably used as a fingerprint in provenance analysis.

Supplementary Materials: The following supporting information can be downloaded at: <https://www.mdpi.com/article/10.3390/geosciences12120442/s1>, File S1: Epidote Standards; File S2: Epidotes Bengal; File S3. Full description of “*epidotefull*” MATLAB™ program; Table S1: Information of the nine standards of epidote-group minerals. Names, labels, localities, and source rocks are indicated (SA, mineral collection of Sergio Andò); Table S2: Chemical composition for all points analysed by SEM-EDS on the nine standards of epidote-group minerals. % Ep = $\text{Fe}^{3+} / (\text{Fe}^{3+} + \text{Al} + \text{Cr}^{3+} - 2)$; % Czo = $(\text{Al} - 2) / (\text{Fe}^{3+} + \text{Al} + \text{Cr}^{3+} - 2)$; $X_{\text{Fe}} = \text{Fe}^{3+} / (\text{Fe}^{3+} + \text{Al})$. Formulas from [26,47]; Table S3: Diagnostic Raman peaks of the six epidote and clinozoisite standards (same points analysed by SEM-EDS); ν = main vibrational mode; $X_{\text{Fe}} = \text{Fe}^{3+} / (\text{Fe}^{3+} + \text{Al})$. Table S4. Key information on the studied cores drilled during IODP Expedition 354 to the Bengal Fan (time scale after [57]); Table S5. Sample information. Full sample identifiers are provided in standard IODP notation and shorter labels used in text and tables. Core depth in metres below sea floor. Grain size determined by wet sieving. Age after [57]; Table S6. Heavy-mineral data. HMC and tHMC = heavy-mineral and transparent-heavy-mineral concentration; n.d. = not determined. The ZTR index (sum of zircon, tourmaline, and rutile over total transparent heavy minerals; [61]) evaluates the durability of the detrital assemblage [60]. The Metasedimentary Minerals Index MMI and the Amphibole Color Index ACI vary from 0 in detritus from low-grade to lowermost medium-grade rocks yielding exclusively chloritoid and blue/green amphibole to 100 in detritus from granulite-facies or volcanic rocks yielding exclusively sillimanite and brown hornblende or oxy-hornblende and are used to estimate the average metamorphic grade of source rocks and provenance of amphibole grains, respectively [59]; Table S7. Compositional variability of epidote-group minerals in 41 samples of Bengal Fan turbidites ranging in grain size from fine silt to medium sand. GSZ, grain size; n° , number of analysed grains; tHM, transparent heavy-minerals, EpGM, epidote-group minerals, Ep, epidote, Czo, clinozoisite, Zo, zoisite, Aln, allanite, RF Ep, epidote-bearing rock fragments; Table S8. Raman peaks in the high-frequency OH region for each studied epidote and clinozoisite grain in Bengal Fan turbidites from core U1454 and corresponding X_{Fe} value estimated by the new MATLAB™ program *epidotefull*; Table S9. Raman peaks in the high-frequency OH region for each studied epidote and clinozoisite grain in Bengal Fan turbidites from core U1453 and corresponding X_{Fe} value estimated by the new MATLAB™ program *epidotefull*; Table S10. Raman peaks in the high-frequency OH region for each studied epidote and clinozoisite grain in Bengal Fan turbidites from core U1452 and corresponding X_{Fe} value estimated by the new MATLAB™ program *epidotefull*; Table S11. Raman peaks in the high-frequency OH region for each studied epidote and clinozoisite grain in Bengal Fan turbidites from core U1449 and corresponding X_{Fe} value estimated by the new MATLAB™ program *epidotefull*; Table S12. Raman peaks in the high-frequency OH region for each studied epidote and clinozoisite grain in Bengal Fan turbidites from core U1451 and corresponding X_{Fe} value estimated by the new MATLAB™ program *epidotefull*; Figure S1: Spectral deconvolution in the OH stretching region of epidote standard E4. A single Gauss-Lorentzian peak was used for each peak, despite its slight asymmetry, to identify a unique band position for the calculation of X_{Fe} values based on Raman spectra with the MATLAB™ routine “*epidotefull*”. The calculations are based on all four main Raman peaks (ν_1 , ν_2 , ν_3 , and ν_4).

Author Contributions: Conceptualization, M.L., S.A. and D.B.; methodology, M.L. and S.A.; software, D.B.; validation, S.A. and D.B.; formal analysis, M.L.; investigation, M.L.; resources, M.L.; data curation, M.L. and S.A.; writing—original draft preparation, M.L. and E.G.; writing—review and editing, M.L. and E.G.; visualization, M.L. and E.G.; supervision, M.L., S.A. and E.G.; project administration, M.L. and S.A.; funding acquisition, M.L. All authors have read and agreed to the published version of the manuscript.

Funding: This research was funded through MUR for ECORD-IODP Italia (<http://www.iodp-italia.cnr.it/index.php/it/opportunita/bandi-cnr-iodp-it/bando-cnr-ecord-iodp-italia-2018>).

Acknowledgments: The studied Bengal Fan samples were obtained thanks to the International Ocean Discovery Program (IODP) and the kind help of Kubo and the technical staff of the IODP Core Repository Kochi Institute for Core Sample Research (<http://www.kochi-core.jp/en/iodp-curation/index.html>). We warmly thank Paolo Gentile for the SEM-EDS analyses and Pietro Vignola, Marco Marchesini, and Alessandro Cavallo for mineralogical advice. This research was funded through MUR for ECORD-IODP Italia (<http://www.iodp-italia.cnr.it/index.php/it/opportunita/bandi-cnr-iodp-it/bando-cnr-ecord-iodp-italia-2018>). We thank the two reviewers for their careful and critical comments.

Conflicts of Interest: The authors declare no conflict of interest.

References

1. Mange, M.A.; Maurer, H.F.W. *Heavy Minerals in Colour*; Chapman & Hall: London, UK, 1992; p. 147.
2. Morton, A.C.; Hallsworth, C.R. Processes controlling the composition of heavy mineral assemblages in sandstones. *Sediment. Geol.* **1999**, *124*, 3–29. [[CrossRef](#)]
3. von Eynatten, H.; Dunkl, I. Assessing the sediment factory: The role of single grain analysis. *Earth Sci. Rev.* **2012**, *115*, 97–120.
4. Worobiec, A.; Stefaniak, E.A.; Potgieter-Vermaak, S.; Sawlowicz, Z.; Spolnik, Z.; Van Grieken, R. Characterisation of concentrates of heavy mineral sands by micro-Raman spectrometry and CC-SEM/EDX with HCA. *Appl. Geochem.* **2007**, *22*, 2078–2085. [[CrossRef](#)]
5. Andò, S.; Garzanti, E. Raman spectroscopy in heavy-mineral studies. *Geol. Soc.* **2014**, *386*, 395–412. [[CrossRef](#)]
6. Delmonte, B.; Paleari, C.I.; Andò, S.; Garzanti, E.; Andersson, P.S.; Petit, J.R.; Crosta, X.; Narcisi, B.; Baroni, C.; Salvatore, M.C.; et al. Causes of dust size variability in central East Antarctica (Dome B): Atmospheric transport from expanded South American sources during Marine Isotope Stage 2. *Quat. Sci. Rev.* **2017**, *168*, 55–68. [[CrossRef](#)]
7. Borromeo, L.; Andò, S.; France-Lanord, C.; Coletti, G.; Hahn, A.; Garzanti, E. Provenance of Bengal shelf sediments: 1. Mineralogy and geochemistry of silt. *Minerals* **2019**, *9*, 640. [[CrossRef](#)]
8. Griffith, W.P. Raman studies on rock-forming minerals. Part I. Orthosilicates and cyclosilicates. *J. Chem. Soc. A Inorg. Phys. Theoret.* **1969**, *192*, 1372–1377. [[CrossRef](#)]
9. Hope, G.A.; Woods, R.; Munce, C.G. Raman microprobe mineral identification. *Miner. Eng.* **2001**, *14*, 1565–1577. [[CrossRef](#)]
10. Bersani, D.; Andò, S.; Vignola, P.; Moltifiori, G.; Marino, I.G.; Lottici, P.P.; Diella, V. Micro-Raman spectroscopy as a routine tool for garnet analysis. *Spectrochim. Acta A Mol. Biomol. Spectrosc.* **2009**, *73*, 484–491. [[CrossRef](#)]
11. Vermeesch, P.; Garzanti, E. Making geological sense of ‘Big Data’ in sedimentary provenance analysis. *Chem. Geol.* **2015**, *409*, 20–27. [[CrossRef](#)]
12. Vermeesch, P.; Rittner, M.; Petrou, E.; Omma, J.; Mattinson, C.; Garzanti, G. High throughput petrochronology and sedimentary provenance analysis by automated phase mapping and LAICPMS. *Geochem. Geophys. Geosystems* **2017**, *18*, 4096–4109. [[CrossRef](#)]
13. Schulz, B.; Gerhard, M.; Jens, G. Automated SEM mineral liberation analysis (MLA) with generically labelled EDX spectra in the mineral processing of rare earth element ores. *Minerals* **2019**, *9*, 527. [[CrossRef](#)]
14. Bersani, D.; Andò, S.; Scrocco, L.; Gentile, P.; Salvioli-Mariani, E.; Fornasini, L.; Lottici, P.P. Composition of amphiboles in the tremolite–ferro–actinolite series by Raman Spectroscopy. *Minerals* **2019**, *9*, 491. [[CrossRef](#)]
15. Borromeo, L.; Andò, S.; Bersani, D.; Garzanti, E.; Gentile, P.; Mantovani, L.; Tribaudino, M. Detrital orthopyroxene as a tracer of geodynamic setting: A Raman and SEM-EDS provenance study. *Chem. Geol.* **2022**, *596*, 120809. [[CrossRef](#)]
16. Heller, B.M.; Lünsdorf, N.K.; Dunkl, I.; Molnár, F.; von Eynatten, H. Estimation of radiation damage in titanites using Raman spectroscopy. *Am. Mineral. J. Earth Planet. Mater.* **2019**, *104*, 857–868. [[CrossRef](#)]
17. Lünsdorf, N.K.; Kalies, J.; Ahlers, P.; Dunkl, I.; von Eynatten, H. Semi-automated heavy-mineral analysis by Raman spectroscopy. *Minerals* **2019**, *9*, 385. [[CrossRef](#)]
18. Liebscher, A. Spectroscopy of epidote minerals. *Rev. Mineral. Geochem.* **2004**, *56*, 125–170. [[CrossRef](#)]
19. Qin, F.; Wu, X.; Wang, Y.; Fan, D.; Qin, S.; Yang, K.; Townsend, J.P.; Jacobsen, S.D. High-pressure behavior of natural single-crystal epidote and clinozoisite up to 40 GPa. *Phys. Chem. Miner.* **2016**, *43*, 649–659. [[CrossRef](#)]
20. Varlamov, D.A.; Ermolaeva, V.N.; Chukanov, N.V.; Jančev, S.; Vigasina, M.F.; Plechov, P.Y. New Data on Epidote-Supergroup Minerals: Unusual Chemical Compositions, Typochemistry, and Raman Spectroscopy. *Geol. Ore Depos.* **2019**, *61*, 827–842. [[CrossRef](#)]
21. Coccato, A.; Bersani, D.; Caggiani, M.C.; Mazzoleni, P.; Barone, G. Raman studies on zoisite and tanzanite for gemmological applications. *J. Raman Spectrosc.* **2021**, *53*, 550–562. [[CrossRef](#)]
22. Spiegel, C.; Siebel, W.; Frisch, W.; Berner, Z. Nd and Sr isotopic ratios and trace element geochemistry of epidote from the Swiss Molasse Basin as provenance indicators: Implications for the reconstruction of the exhumation history of the Central Alps. *Chem. Geol.* **2002**, *189*, 231–250. [[CrossRef](#)]
23. Liang, W.; Garzanti, E.; Andò, S.; Gentile, P.; Resentini, A. Multimineral fingerprinting of Transhimalayan and Himalayan sources of Indus-derived Thal Desert sand (central Pakistan). *Minerals* **2019**, *9*, 457. [[CrossRef](#)]
24. Huber, B.; Bahlburg, H. The provenance signal of climate–tectonic interactions in the evolving St. Elias orogen: Framework component analysis and pyroxene and epidote single grain geochemistry of sediments from IODP 341 sites U1417 and U1418. *Int. J. Earth Sci.* **2021**, *110*, 1477–1499. [[CrossRef](#)]
25. Frei, D.; Liebscher, A.; Franz, G.; Dulski, P. Trace element geochemistry of epidote minerals. *Rev. Mineral. Geochem.* **2004**, *56*, 553–605. [[CrossRef](#)]
26. Enami, M.; Liou, J.G.; Mattinson, C.G. Epidote minerals in high P/T metamorphic terranes: Subduction zone and high-to ultrahigh-pressure metamorphism. *Rev. Mineral. Geochem.* **2004**, *56*, 347–398. [[CrossRef](#)]
27. Grapes, R.H.; Hoskin, P.W. Epidote group minerals in low–medium pressure metamorphic terranes. *Rev. Mineral. Geochem.* **2004**, *56*, 301–345. [[CrossRef](#)]
28. Mange, M.A.; Morton, A.C. Geochemistry of heavy minerals. In *Developments in Sedimentology*; Mange, M., Wright, D.T., Eds.; Elsevier: Amsterdam, The Netherlands, 2007; Volume 58, pp. 345–391.

29. Armbruster, T.; Bonazzi, P.; Akasaka, M.; Bermanec, V.; Chopin, C.; Gieré, R.; Heuss-Assbichler, S.; Liebscher, A.; Menchetti, S.; Pan, Y.; et al. Recommended nomenclature of epidote-group minerals. *Eur. J. Mineral.* **2006**, *18*, 551–567. [[CrossRef](#)]
30. Garzanti, E.; Andò, S. Plate tectonics and heavy mineral suites of modern sands. In *Developments in Sedimentology*; Mange, M., Wright, D.T., Eds.; Elsevier: Amsterdam, The Netherlands, 2007; Volume 58, pp. 741–763.
31. Milliken, K.L. Provenance and diagenesis of heavy minerals, Cenozoic units of the northwestern Gulf of Mexico sedimentary basin. In *Developments in Sedimentology*; Mange, M., Wright, D.T., Eds.; Elsevier: Amsterdam, The Netherlands, 2007; Volume 58, pp. 247–261.
32. Morton, A.C.; Hallsworth, C. Stability of detrital heavy minerals during burial diagenesis. In *Developments in Sedimentology*; Mange, M., Wright, D.T., Eds.; Elsevier: Amsterdam, The Netherlands, 2007; Volume 58, pp. 215–245.
33. Limonta, M.; Resentini, A.; Carter, A.; Bandopadhyay, P.C.; Garzanti, E. Provenance of Oligocene Andaman sandstones (Andaman–Nicobar Islands): Ganga–Brahmaputra or Irrawaddy derived? *Geol. Soc. Lond. Mem.* **2017**, *47*, 141–152. [[CrossRef](#)]
34. Garzanti, E.; Andò, S.; Limonta, M.; Fielding, L.; Najman, Y. Diagenetic control on mineralogical suites in sand, silt, and mud (Cenozoic Nile Delta): Implications for provenance reconstructions. *Earth Sci. Rev.* **2018**, *185*, 122–139. [[CrossRef](#)]
35. Garzanti, E.; Andò, S. Heavy mineral concentration in modern sands: Implications for provenance interpretation. In *Developments in Sedimentology*; Mange, M., Wright, D.T., Eds.; Elsevier: Amsterdam, The Netherlands, 2007; Volume 58, pp. 517–545.
36. Gottschalk, M. Thermodynamic properties of zoisite, clinozoisite and epidote. *Rev. Mineral. Geochem.* **2004**, *56*, 83–124. [[CrossRef](#)]
37. Schmidt, M.W.; Poli, S. Magmatic epidote. *Rev. Mineral. Geochem.* **2004**, *56*, 399–430. [[CrossRef](#)]
38. Deer, W.A.; Howie, R.A.; Zussman, J. (Eds.) *Rock-Forming Minerals: Disilicates and Ring Silicates*, 2nd ed.; Geological Society: London, UK, 1997; Volume 1B.
39. Pichler, H.; Schmitt-Riegraf, C. *Rock-Forming Minerals in Thin Section*; Springer Science & Business Media: Berlin/Heidelberg, Germany, 1997.
40. Exley, R.A. Microprobe studies of REE-rich accessory minerals: Implications for Skye granite petrogenesis and REE mobility in hydrothermal systems. *Earth Planet. Sci. Lett.* **1980**, *48*, 97–110. [[CrossRef](#)]
41. Brooks, C.K.; Henderson, P.; Rønsbo, J.G. Rare-earth partition between allanite and glass in the obsidian of Sandy Braes, Northern Ireland. *Mineral. Mag.* **1981**, *44*, 157–160. [[CrossRef](#)]
42. Gromet, L.P.; Silver, L.T. Rare earth element distributions among minerals in a granodiorite and their petrogenetic implications. *Geochim. Cosmochim. Acta* **1983**, *47*, 925–939. [[CrossRef](#)]
43. Ercit, T.S. The mess that is “allanite”. *Can. Mineral.* **2002**, *40*, 1411–1419. [[CrossRef](#)]
44. Gieré, R.; Sorensen, S.S. Allanite and other REE-rich epidote-group minerals. *Rev. Mineral. Geochem.* **2004**, *56*, 431–493. [[CrossRef](#)]
45. Dunkl, I.; von Eynatten, H.; Andò, S.; Lünsdorf, K.; Morton, A.; Alexander, B.; Aradi, L.; Augustsson, C.; Bahlburg, H.; Barbarano, M.; et al. Comparability of heavy mineral data—The first interlaboratory round robin test. *Earth Sci. Rev.* **2020**, *211*, 103210. [[CrossRef](#)]
46. Winkler, H.G.F. *Petrogenesis of Metamorphic Rocks*; Springer: New York, NY, USA, 1976; p. 334.
47. Franz, G.; Liebscher, A. Physical and Chemical Properties of the Epidote Minerals—An Introduction. *Rev. Mineral. Geochem.* **2004**, *56*, 1–81. [[CrossRef](#)]
48. Hörmann, P.K.; Raith, M. Optische Daten, Gitterkonstanten, Dichte und magnetische Suszeptibilität von Al-Fe (III)-Epidoten. *N. Jahrb. Mineral. Abh.* **1971**, *116*, 41–60.
49. Wang, A.; Han, J.; Guo, L.; Yu, J.; Zeng, P. Database of standard Raman spectra of minerals and related inorganic crystals. *Appl. Spectrosc.* **1994**, *48*, 959–968. [[CrossRef](#)]
50. Huang, E. Raman spectroscopic study of 15 gem minerals. *J. Geol. Soc. China* **1999**, *42*, 301–318.
51. Nagashima, M.; Armbruster, T.; Nishio-Hamane, D.; Mihailova, B. The structural state of Finnish Cr- and V-bearing clinozoisite: Insights from Raman spectroscopy. *Phys. Chem. Miner.* **2021**, *48*, 1–14. [[CrossRef](#)]
52. Antofilli, M.; Borgo, E.; Palenzona, A. *I Nostri Minerali. Geologia e Mineralogia in Liguria*; SAGEP Editrice: Genova, Italia, 1985.
53. Seemann, R. Famous mineral localities: Knappenwand, Untersulzbachtal (Austria). *Mineral. Rec.* **1986**, *17*, 167–181.
54. Bedogné, F.; Montrasio, A.; Sciesa, E. *I Minerali della Provincia di Sondrio: Valmalenco*; Bettini: Sondrio, Italia, 1993; p. 275.
55. Piccoli, G.C.; Maletto, G.; Bosio, P.; Lombardo, B. *Minerali del Piemonte e della Valle d’Aosta*; L’Artigiana: Alba, Italy, 2007; p. 607.
56. Marty, F. The Trimouns quarry, Luzenac, Ariège, France. *Mineral. Rec.* **2004**, *35*, 225–247.
57. France-Lanord, C.; Spiess, V.; Klaus, A.; Schwenk, T.; Adhikari, T.T.; Adhikari, S.K.; Bahk, J.J.; Baxter, A.T.; Cruz, J.W.; Das, S.K.; et al. Expedition 354 summary. In *International Ocean Discovery Program 354 Preliminary Report*; IODP: College Station, TX, USA, 2016; pp. 1–35.
58. Andò, S. *Heavy Minerals: Methods & Case Histories*; MDPI: Basel, Switzerland, 2020.
59. Garzanti, E.; Andò, S. Heavy minerals for junior woodchucks. *Minerals* **2019**, *9*, 148. [[CrossRef](#)]
60. Garzanti, E. The maturity myth in sedimentology and provenance analysis. *J. Sediment. Res.* **2017**, *87*, 353–365. [[CrossRef](#)]
61. Hubert, J.F. A zircon-tourmaline-rutile maturity index and the interdependence of the composition of heavy mineral assemblages with the gross composition and texture of sandstones. *J. Sediment. Petrol.* **1962**, *32*, 440–450.
62. Limonta, M.; Garzanti, E.; Resentini, A. Petrology of Bengal Fan turbidites (IODP Expeditions 353 and 354): Provenance versus diagenetic control. *J. Sediment. Res.* **2023**; in press.

-
63. Tröger, W.E. *Optical determination of rock-forming minerals, Part I*; Bambauer, H.U., Ed.; Schweizerbart Science Publishers: Stuttgart, Germany, 1979.
 64. Makreski, P.; Jovanovski, G.; Kaitner, B.; Gajović, A.; Biljan, T. Minerals from Macedonia. *Vib. Spectrosc.* **2007**, *1*, 162–170. [[CrossRef](#)]